45th AIAA Aerospace Sciences Meeting and Exhibit
8 - 11 January 2007, Reno, Nevada

AIAA 2007-1415

45th AIAA Aerospace Sciences Meeting, Jan 8–11, Reno,Nevada

An Algorithm for DNS/LES of Compressible Reacting Flows

Jeff Doom* and Krishnan Mahesh†
University of Minnesota, Minneapolis, MN, 55455, USA

A non–dissipative, implicit, all Mach number algorithm for direct numerical and large eddy simulation of compressible reacting flows, is described. The compressible Navier–Stokes equations are rescaled so that the zero Mach number reacting equations are discretely recovered in the limit of zero Mach number. The dependent variables are co–located in space, and thermodynamic variables are staggered from velocity in time. The algorithm discretely conserves kinetic energy in the incompressible, inviscid, non–reacting limit. The species equations are implicit to allow for stiff chemical mechanisms, and are readily applied to complex chemistry. Numerical examples ranging from one–step chemistry to a nine species, nineteen reaction mechanism for H2 and O2 are presented.

I. Introduction

The direct numerical simulation (DNS) and large–eddy simulation (LES) of turbulent reacting flows are extremely challenging. Combustion involves a large number of chemical species, and associated chemical reactions. Different chemical reactions possess different time–scales, and different reaction zone thicknesses. Turbulence introduces its own range of length and time–scales. Turbulent combustion can occur at very low Mach numbers (e.g. gas–turbine combustors at low pressures) or very high Mach numbers (e.g. scramjets). Very low Mach numbers imply numerical stiffness because of a large difference between the speed of sound and flow velocities, while very high Mach numbers result in shock waves, and their attendant problems. Therefore, the desired requirements for direct numerical simulation and large eddy simulation for reacting compressible flows are: i) the ability to simulate compressible reacting flows without loss of robustness and accuracy at high Reynolds numbers, ii) the ability to effectively compute flows in both subsonic and supersonic regions, iii) the ability to handle stiffness resulting from chemical mechanisms, and iv) accurately simulate flows with shocks. This paper presently addresses the first three requirements.

Most DNS/LES of turbulent reacting flows appear to either use the compressible Navier–Stokes equations with Pade spatial discretization, and explicit time–advancement (e.g. Poinsot[4] –,[6] Lele,[7] Pantano[8]), or the zero Mach number equations along with a pressure–projection approach (e.g. Majda & Sethian,[9] Montgomery & Riley,[10] Rutland & Ferziger[11]–,[12] Pierce & Moin,[13] Pember et al,[14] Mahesh et al.[15]). However, the Pade schemes become unstable at high Reynolds numbers; when explicit time–advancement is used, they require very small time–step at low Mach numbers, and for stiff chemical mechanisms. The zero Mach number equations are very efficient at low Mach numbers because they analytically project acoustic waves out; also along with implicit time–advancement they can resolve chemical stiffness efficiently. However, due to the complete absence of acoustic effects, they are not applicable to finite Mach number flows.

*Graduate Research Assistant
†Associate Professor

This paper therefore extends the non–reacting Hou & Mahesh[1] algorithm to include the effects of chemical reaction. The resulting algorithm treats the chemical source terms implicitly, solves the species equations in a segregated manner, which allows easy extension to multiple species and chemical reactions, and reduces to the zero Mach number equations in the limit of very small Mach number. The paper is organized as follows. Section II describes the non–dimensional governing equations, and their behavior in the limit of very small Mach number. The discrete scheme is described in section III. The positioning of variables, and details of the pressure–correction approach are discussed. Section IV presents some numerical examples. Results are shown for a laminar premixed flame, laminar unstrained diffusion flame, laminar reacting two–dimensional jet, a turbulent non–premixed flame and an extension to complex chemistry incorporating a H2–O2 nine species, nineteen reaction mechanism. A brief summary in section V concludes the paper.

II. Governing Equations

The governing equations are the compressible, reacting Navier–Stokes equation for an ideal gas:

$$\frac{\partial \rho^d}{\partial t^d} + \frac{\partial \rho u_j^d}{\partial x_j^d} = 0, \tag{1}$$

$$\frac{\partial \rho^d Y_k^d}{\partial t^d} + \frac{\partial \rho Y_k^d u_j^d}{\partial x_j^d} = \frac{\partial}{\partial x_j^d}\left(\rho^d D_k^d \frac{\partial Y_k^d}{\partial x_j^d}\right) + \dot{\omega}_k^d, \tag{2}$$

$$\frac{\partial \rho^d u_i^d}{\partial t^d} + \frac{\partial \rho^d u_i^d u_j^d}{\partial x_j^d} = -\frac{\partial p^d}{\partial x_i^d} + \frac{\partial \tau_{ij}^d}{\partial x_j^d}, \tag{3}$$

$$\frac{\partial \rho^d E^d}{\partial t^d} + \frac{\partial \left(\rho^d E^d + p^d\right) u_j^d}{\partial x_j^d} = \frac{\partial \tau_{ij}^d u_i^d}{\partial x_j^d} + \frac{\partial}{\partial x_j^d}\left(\mu^d \frac{c_p^d}{Pr}\frac{\partial T^d}{\partial x_j^d}\right) + \sum_{k=1}^{N} Q_k^d \dot{\omega}_k^d \tag{4}$$

$$p^d = \rho^d R T^d. \tag{5}$$

where the superscript 'd' denotes the dimensional value. The variables ρ, p, Y_k and u_i denote the density, pressure, mass fraction of species k and velocities respectively. $E = c_v T^d + u_i^d u_i^d/2$ denotes the total energy per unit mass and $\tau_{ij} = \mu^d\left(\frac{\partial u_i^d}{\partial x_j^d} + \frac{\partial u_j^d}{\partial x_i^d} - \frac{2}{3}\frac{\partial u_k^d}{\partial x_k^d}\delta_{ij}\right)$ is the viscous stress tensor. D_k^d, c_p, and Pr denote the diffusion coefficient of the k^{th} species, specific heat at constant pressure, and the Prandtl number. For the source term, Q_n^d is the heat of reaction per unit mass and $Q_n^d \dot{\omega}_n^d$ is the heat release due to combustion for the 'n^{th}' reaction. $\dot{\omega}_k$ is the mass reaction rate for the k^{th} species. The source term is modeled using the Arrhenius law in this paper.

The reacting governing equation are non–dimensionalized as follows. Let ρ_r, Y_r, L, & T_r denote the reference density, mass fraction, length and temperature respectively. The reference velocity, dynamic viscosity and pressure are denoted by u_r, μ_r and p_r respectively. This yields the following non–dimensional variables:

$$\rho = \frac{\rho^d}{\rho_r}, \quad u_i = \frac{u_i^d}{u_r}, \quad t = \frac{t^d}{L/u_r}, \quad \mu = \frac{\mu^d}{\mu_r}, \quad p = \frac{p^d - p_r}{\rho_r {u_r}^2}, \tag{6}$$

$$T = \frac{T^d}{T_r}, \quad M_r = \frac{u_r}{a_r} = \frac{u_r}{\sqrt{\gamma R T_r}}, \tag{7}$$

$$Y_k = \frac{Y_k^d}{Y_r}, \quad D_k = \frac{D_k^d}{u_r L}, \quad \dot{\omega}_k = \frac{L\dot{\omega}_k^d}{u_r \rho_r Y_r} \quad \text{and} \quad Q_n = \frac{Y_r Q_n^d}{c_p T_r}. \tag{8}$$

Note that pressure is non–dimensionalized using an incompressible scaling. This non–dimensionalization is motivated by Thompson,[2] Bijl & Wesseling,[3] Van der Heul et al.[16] and Hou & Mahesh.[1] Therefore, the non–dimensional governing equations for reacting flows are:

$$\frac{\partial \rho}{\partial t} + \frac{\partial \rho u_j}{\partial x_j} = 0, \tag{9}$$

$$\frac{\partial \rho Y_k}{\partial t} + \frac{\partial \rho Y_k u_j}{\partial x_j} = \frac{1}{ReSc_k}\frac{\partial}{\partial x_j}\left(\mu \frac{\partial Y_k}{\partial x_j}\right) + \dot{\omega}_k, \tag{10}$$

$$\frac{\partial \rho u_i}{\partial t} + \frac{\partial \rho u_i u_j}{\partial x_j} = -\frac{\partial p}{\partial x_i} + \frac{1}{Re}\frac{\partial \tau_{ij}}{\partial x_j}, \tag{11}$$

$$M_r^2\left[\frac{\partial}{\partial t}\left(p + \frac{\gamma-1}{2}\rho u_i u_i\right) + \frac{\partial}{\partial x_j}\left(\gamma p + \frac{\gamma-1}{2}\rho u_i u_i\right)u_j\right] + \frac{\partial u_j}{\partial x_j}$$
$$= \frac{(\gamma-1)M_r^2}{Re}\frac{\partial \tau_{ij} u_i}{\partial x_j} + \frac{1}{RePr}\frac{\partial}{\partial x_j}\left(\mu \frac{\partial T}{\partial x_j}\right) + \sum_{k=1}^{N} Q_k \dot{\omega}_k. \tag{12}$$

$$\rho T = \gamma M_r^2 p + 1 \tag{13}$$

where Sc_k is the Schmidt number for the k^{th} species. When the Mach number is zero, the non-dimensional reacting governing equations reduce to:

$$\frac{\partial \rho}{\partial t} + \frac{\partial \rho u_j}{\partial x_j} = 0, \tag{14}$$

$$\frac{\partial \rho u_i}{\partial t} + \frac{\partial \rho u_i u_j}{\partial x_j} = -\frac{\partial p}{\partial x_i} + \frac{1}{Re}\frac{\partial \tau_{ij}}{\partial x_j}, \tag{15}$$

$$\frac{\partial \rho Y_k}{\partial t} + \frac{\partial \rho Y_k u_j}{\partial x_j} = \frac{1}{ReSc_k}\frac{\partial}{\partial x_j}\left(\mu \frac{\partial Y_k}{\partial x_j}\right) + \dot{\omega}_k, \tag{16}$$

$$\frac{\partial u_j}{\partial x_j} = \frac{1}{RePr}\frac{\partial}{\partial x_j}\left(\mu \frac{\partial T}{\partial x_j}\right) + \sum_{k=1}^{N} Q_k \dot{\omega}_k, \tag{17}$$

$$\rho T = 1. \tag{18}$$

Notice that the divergence of velocity equals the sum of the terms involving thermal conduction and heat release. If the density is constant and there is no heat release, the energy equation reduces to the incompressible continuity equation. In the presence of heat release, the zero Mach number reacting equations (Majda & Sethian[9]) are obtained. Most projection methods for the zero Mach number equations project the momentum ρu_i to satisfy the momentum equation. Here, the velocity is projected to satisfy the energy equation. The reaction source term can be quite complicated for multiple species, and is discussed in more detail in section A.

III. Discretization

Density, pressure, and temperature are staggered in time from velocity by Hou and Mahesh [3]. The mass fraction of species k are similarly staggered in time here. The thermodynamic variables and mass fraction of species k are advanced in time from $t + \frac{1}{2}$ to $t + \frac{3}{2}$, illustrated in figure 1. The variables are co–located in space, to allow easy application to unstructured grids.

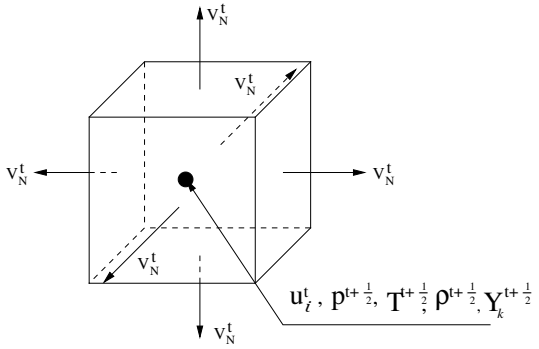

Figure 1. Storage of variables.

Integrating over the control volume and applying Gauss's theorem yields the discrete governing equations. The discrete continuity and species equations are

$$\frac{\rho_{cv}^{t+\frac{3}{2}} - \rho_{cv}^{t+\frac{1}{2}}}{\Delta t} + \frac{1}{V}\sum_{faces} \rho_{faces}^{t+1} V_N^{t+1} A_{face} = 0 \tag{19}$$

and

$$\frac{(S_k)_{cv}^{t+\frac{3}{2}} - (S_k)_{cv}^{t+\frac{1}{2}}}{\Delta t} + \frac{1}{V}\sum_{faces} (S_k)_{faces}^{t+1} V_N^{t+1} A_{face}$$
$$= \frac{1}{ReSc_k}\frac{1}{V}\sum_{faces}\left(\mu\left[\frac{1}{\rho}\frac{\partial S_k}{\partial x_j} - \frac{S_k}{\rho^2}\frac{\partial \rho}{\partial x_j}\right]\right)_{faces}^{t+1} N_j A_{face} + \dot{\omega}_k^{t+1}. \tag{20}$$

where ρ_{cv} denotes $\rho_{i,j,k}$ and $\sum_{faces}$ denotes summation over all the faces of the control volume. ρ_{faces} and v_N denotes the density and normal face velocity at each face. Note that $S_k = \rho Y_k$. The variables $(S_k)_{faces}$ denotes the species at the face and N_j is the outward normal vector at the face. The variables V and A_{face} denote the volume of the control volume and the area of the face. The discrete momentum equation is:

$$\frac{(g_i)_{cv}^{t+1} - (g_i)_{cv}^{t}}{\Delta t} + \frac{1}{V}\sum_{faces} (g_i)_{faces}^{t+\frac{1}{2}} V_N^{t+\frac{1}{2}} A_{face}$$
$$= -\frac{1}{V}\sum_{faces} p_{faces}^{t} N_j A_{face} + \frac{1}{Re}\frac{1}{V}\sum_{faces} (\tau_{ij})_{face}^{t+\frac{1}{2}} N_j A_{face}. \tag{21}$$

Here, $g_i = \rho u_i$ denotes the momentum in the i direction and τ_{ij} is the stress tensor. The discrete energy equation is given by:

$$M_r^2\left[\frac{\partial}{\partial t}\left(p_{cv} + \frac{\gamma-1}{2}\rho u_i u_i\right)^{t+\frac{1}{2}} + \frac{1}{V}\sum_{faces}\left(\gamma p_{cv} + \frac{\gamma-1}{2}\rho u_i u_i\right)_{face}^{t+\frac{1}{2}} \cdot v_N^{t+\frac{1}{2}} A_{face}\right]$$
$$+\frac{1}{V}\sum_{face} v_N^{t+\frac{1}{2}} A_{face} = \frac{(\gamma-1)M_r^2}{Re}\frac{1}{V}\sum_{faces} (\tau_{ij}u_i)_{face}^{t+\frac{1}{2}} N_j A_{face}$$
$$+\frac{1}{RePr}\frac{1}{V}\sum_{faces}\left(\mu\frac{\partial T^{t+\frac{1}{2}}}{\partial N}\right) A_{face} + \sum_{n=1}^{M} Q_n \dot{\omega}_n^{t+\frac{1}{2}}. \tag{22}$$

The algorithm solves each equation separately. This allows one to add multiple species with relative ease, which allows easy extension to complex chemistry. Note that the chemical source term is handled implicitly. Details of the implicit procedure are described in section A. The algorithm is a pressure–correction method. An important feature is that the face–normal velocities are projected to satisfy the constraint on the divergence which is determined by the energy equation. At small Mach number, this feature ensures that the velocity field is discretely divergence free. This is in contrast to most approaches that project the momentum which is constrained by the continuity equation. A predictor–corrector approach is used to solve the momentum and energy equation:

$$p^{t+\frac{3}{2},k+1} = p^{t+\frac{3}{2},k} + \delta p. \tag{23}$$

The corrector step is the difference between the predictor equation and the exact equation which is defined as:

$$g_{i,cv}^{t+1,k+1} = g_{i,cv}^{*} - \frac{\Delta t}{4}\left(\frac{\partial \delta p}{\partial x_i}\right)_{cv}, \tag{24}$$

$$u_{i,cv}^{t+1,k+1} = u_{i,cv}^{*} - \frac{\Delta t}{4\rho_{cv}^{t+1}}\left(\frac{\partial \delta p}{\partial x_i}\right)_{cv}. \tag{25}$$

Substituting equation (25) into the nonlinear term $u_i u_i$ converts kinetic energy into an equation for δp which is:

$$\begin{aligned}\left(u_i u_i\right)^{t+1,k+1} &= \left(u_i^{*} - \frac{\Delta t}{4\rho_{cv}^{t+1}}\left(\frac{\partial \delta p}{\partial x_i}\right)\right)\left(u_i^{*} - \frac{\Delta t}{4\rho_{cv}^{t+1}}\left(\frac{\partial \delta p}{\partial x_i}\right)\right) \\ &= u_i^{*}u_i^{*} - \frac{\Delta t}{2\rho^{t+1}}u_i^{*}\frac{\partial \delta p}{\partial x_i} + O(\delta p^2).\end{aligned} \tag{26}$$

Equation (26) is then substituted into equation (22), and yields a discrete energy equation in terms of δp. Note that δp is the difference between iterations, which implies that δp converges to zero at each time–step. This allows the high order terms in equation (26) to be neglected.

The implementation to solve the following discrete equations are to initialize the outer loop:

$$\rho^{t+\frac{3}{2},0} = \rho^{t+\frac{1}{2}}, \quad u_i^{t+1,0} = u_i^{t}, \quad T^{t+\frac{3}{2},0} = T^{t+\frac{1}{2}}, \quad v_N^{t+1,0} = v_N^{t}, \quad S_k^{t+\frac{3}{2},0} = S_k^{t+\frac{1}{2}}. \tag{27}$$

The next procedure is to advance the continuity equation (19), and then advance the species equation (20). Once the species is advanced, advance the momentum equation (21), then obtain $v_N^{\star}$ by interpolation. After obtaining $v_N^{\star}$, the next step is to solve the pressure correction equation (22). Use the corrector steps to update pressure (23), momentum (24) and the velocities (25), then check the convergence for the pressure, momentum, density, and species between outer loop iterations.

A. Implicit source term

Consider a chemical system of N species reacting through M reactions denoted as (Poinsot & Veynante[5]):

$$\sum_{j=1}^{N} \nu_{kj}' \mu_k \rightleftharpoons \sum_{j=1}^{M} \nu_{kj}'' \mu_k \tag{28}$$

for $j = 1, M$ where μ_k is a symbol for species k. ν_{kj}' and $\nu_{kj}''$are the stoichiometric coefficients of species k for j reactions. The reaction term is defined as:

$$\dot{\omega}_k = W_k \sum_{j=1}^{M} \nu_{kj}\hat{Q}_j \tag{29}$$

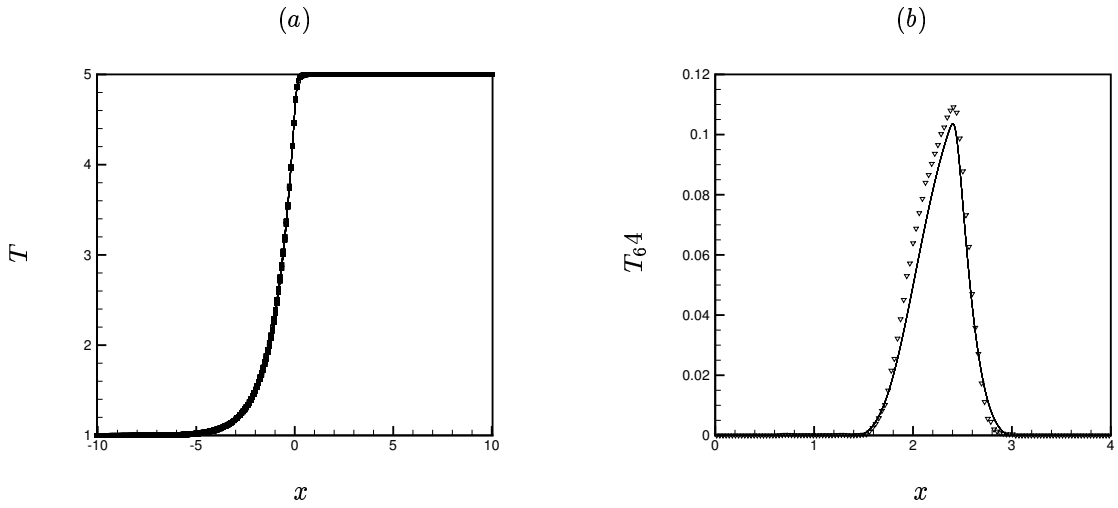

Figure 2. (a) is a comparison of computed solution to analytical solution for a laminar premixed flame. $\beta = 10$, $\alpha = 0.8$, $Sc = Re = Pr = 1$, $M_r = 0.01$. □ **analytic solution,** —— **numerical solution. (b) is a comparison of the asymptotic solution to the numerical solution for a laminar diffusion flame comparing temperature profiles at a non–dimensional time of 64.** □ **asymptotic solution,** —— **numerical solution,** $Sc_k = 1$, $Pr = 1$, $M_r = 0.001$.

where

$$\hat{Q}_j = \underbrace{K_{ij} \prod_{k=1}^{N} \left(\frac{\rho Y_k}{W_k} \right)^{\nu'_{kj}}}_{\text{forward reaction}} - \underbrace{K_{rj} \prod_{k=1}^{N} \left(\frac{\rho Y_k}{W_k} \right)^{\nu''_{kj}}}_{\text{reverse reaction}}. \tag{30}$$

Using the empirical Arrhenius law,

$$K_{ij} = A_{ij} T^{\beta_j} \exp\left(-\frac{E_j}{RT} \right) = A_{ij} T^{\beta_j} \exp\left(-\frac{T_{a_j}}{T} \right). \tag{31}$$

Therefore, the source term is:

$$\begin{aligned} \dot{\omega}_k = W_k \sum_{j=1}^{M} \nu_{kj} \left[A_{ij} T^{\beta_j} \exp\left(-\frac{T_{a_j}}{T} \right) \prod_{k=1}^{N} \left(\frac{S_k}{W_k} \right)^{\nu'_{kj}} \right] \\ - W_k \sum_{j=1}^{M} \nu_{kj} \left[A_{rj} T^{\beta_j} \exp\left(-\frac{T_{a_j}}{T} \right) \prod_{k=1}^{N} \left(\frac{S_k}{W_k} \right)^{\nu''_{kj}} \right]. \end{aligned} \tag{32}$$

The discrete form of equation 32 is:

$$\begin{aligned} \dot{\omega}_k^{t+1} = W_k \sum_{j=1}^{M} \nu_{kj} \left[A_{ij} T_{cv}^{\beta_j, t+1} \exp\left(-\frac{T_{a_j}}{T_{cv}^{t+1}} \right) \prod_{k=1}^{N} \left(\frac{S_{k,cv}^{t+\frac{3}{2}} + S_{k,cv}^{t+\frac{1}{2}}}{2W_k} \right)^{\nu'_{kj}} \right] \\ - W_k \sum_{j=1}^{M} \nu_{kj} \left[A_{rj} T_{cv}^{\beta_j, t+1} \exp\left(-\frac{T_{a_j}}{T_{cv}^{t+1}} \right) \prod_{k=1}^{N} \left(\frac{S_{k,cv}^{t+\frac{3}{2}} + S_{k,cv}^{t+\frac{1}{2}}}{2W_k} \right)^{\nu''_{kj}} \right]. \end{aligned} \tag{33}$$

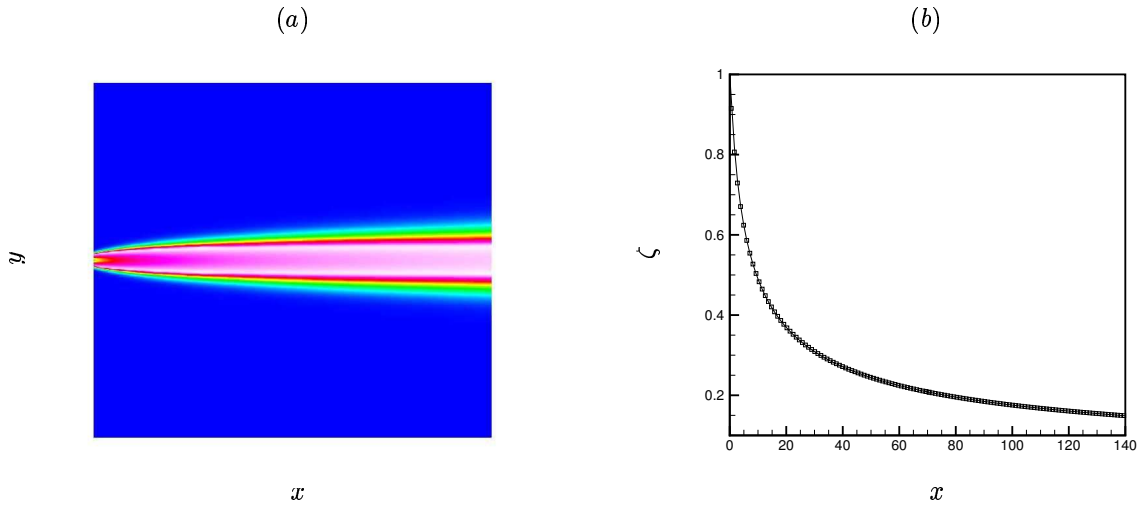

Figure 3. (a) is contour plot of temperature for a diffusion jet flame. (b) is the center line profile of the mixture fraction ζ. □ asymptotic solution from Poinsot & Veynante,[4] ——— numerical solution. $Re = 500$, $Sc_k = Pr = 1$, $M_r = 0.01$.

Substituting equation (33) into equation (20) for $\dot{\omega}_k^{t+1}$ yields:

$$\begin{aligned}
&\frac{(S_k)_{cv}^{t+\frac{3}{2}} - (S_k)_{cv}^{t+\frac{1}{2}}}{\Delta t} + \frac{1}{V}\sum_{faces}(S_k)_{faces}^{t+1} V_N^{t+1} A_{face} \\
&= \frac{1}{ReSc_k}\frac{1}{V}\sum_{faces}\left(\mu\left[\frac{1}{\rho}\frac{\partial S_k}{\partial x_j} - \frac{S_k}{\rho^2}\frac{\partial \rho}{\partial x_j}\right]\right)_{faces}^{t+1} N_j A_{face} \\
&+ W_k \sum_{j=1}^{M}\nu_{kj}\left[A_{ij}T_{cv}^{\beta_j,t+1}\exp\left(-\frac{T_{a_j}}{T_{cv}^{t+1}}\right)\prod_{k=1}^{N}\left(\frac{S_{k,cv}^{t+\frac{3}{2}} + S_{k,cv}^{t+\frac{1}{2}}}{2W_k}\right)^{\nu'_{kj}}\right] \\
&- W_k \sum_{j=1}^{M}\nu_{kj}\left[A_{rj}T_{cv}^{\beta_j,t+1}\exp\left(-\frac{T_{a_j}}{T_{cv}^{t+1}}\right)\prod_{k=1}^{N}\left(\frac{S_{k,cv}^{t+\frac{3}{2}} + S_{k,cv}^{t+\frac{1}{2}}}{2W_k}\right)^{\nu''_{kj}}\right].
\end{aligned} \tag{34}$$

Equation (34) can be represented as:

$$a_p S_{cv}^{t+\frac{3}{2}} + \sum_{nb} a_{nb} S_{nb}^{t+\frac{3}{2}} = RHS. \tag{35}$$

where nb are the neighbors of the cv. A parallel, algebraic multi–grid approach is used to solve the system of algebraic equations. The structured grid interface of the *Hypre* library (Lawrence Livermore National Laboratory 2003) is used.

Two examples will illustrate how to handle the source term if it is either linear or nonlinear. If the stoichiometric coefficients are one, then the source term is linear. For example, consider a two–step reaction from Chen[22] and Mahalingam[20] where the stoichiometric coefficients are one. The reaction mechanism is given by:

$$\begin{aligned}
A + B &\rightarrow I \\
A + I &\rightarrow P.
\end{aligned} \tag{36}$$

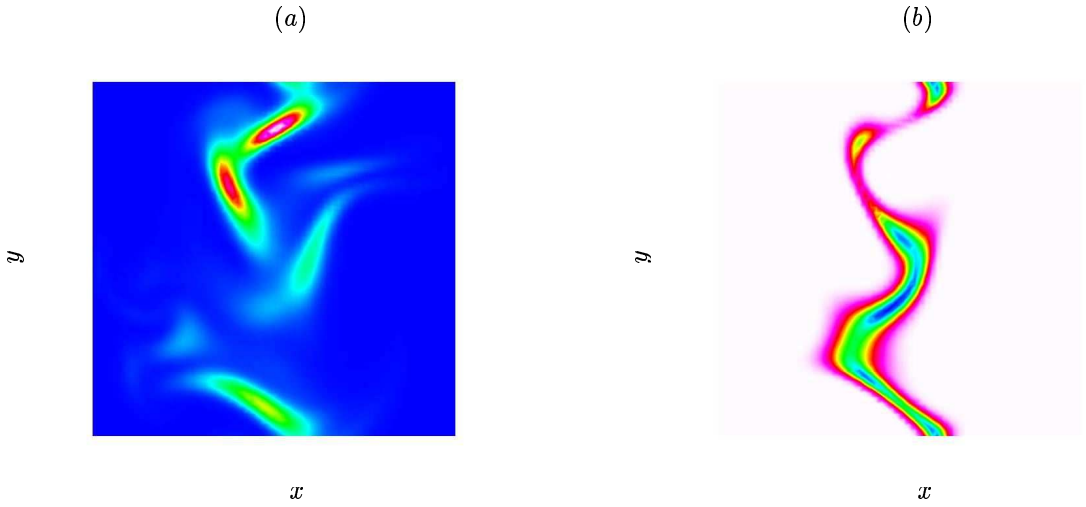

Figure 4. Part (a) is the scalar dissipation rate χ and part (b) is the reaction rate $\dot{\omega}$ at $z = 4$. Notice that scalar dissipation is high where the reaction rate is low. Holes occur where the reaction rate is low which is from Chen & Mahalingam. $Re = 935$, $Sc_k = Pr = 1$, $M_r = 0.1$.

Here A is the fuel, B is the oxidizer, I is the intermediate step, and P is the product. The source term for species A is defined as:

$$\dot{\omega}_k = B_1 \rho Y_A \rho Y_B \exp\left(-\frac{T_{a_1}}{T}\right) + B_2 \rho Y_A \rho Y_I \exp\left(-\frac{T_{a_2}}{T}\right). \tag{37}$$

The discrete form is:

$$\begin{aligned}\dot{\omega}_k = {} & B_1 \frac{S_{A,cv}^{t+\frac{3}{2}} + S_{A,cv}^{t+\frac{1}{2}}}{2} S_{B,cv}^{t+1} \exp\left(-\frac{T_{a_1}}{T_{cv}^{t+1}}\right) \\ & + B_2 \frac{S_{A,cv}^{t+\frac{3}{2}} + S_{A,cv}^{t+\frac{1}{2}}}{2} S_{I,cv}^{t+1} \exp\left(-\frac{T_{a_2}}{T_{cv}^{t+1}}\right).\end{aligned} \tag{38}$$

This implicit source term is used in section C. Note that the other species are handled in a similar manner.

The second example handles the source term if it is nonlinear. Consider one–step reaction used in section IV A and B denoted as:

$$\dot{\omega}_k = -A \rho^{\nu_F + \nu_O} Y_F^{\nu_F} Y_O^{\nu_O} \exp\left(-\frac{T_a}{T}\right). \tag{39}$$

Let $\nu_F = 2$ and $\nu_O = 1$. This implies:

$$\dot{\omega}_k = -A \rho^{2+1} Y_F^2 Y_O^1 \exp\left(-\frac{T_a}{T}\right) = -A S_F^2 S_O^1 \exp\left(-\frac{T_a}{T}\right) \tag{40}$$

where F is the fuel and O is the oxidizer. The discrete equation for the fuel species is:

$$\dot{\omega}_k^{t+1} = -A \underbrace{\left[\frac{S_{F,cv}^{t+\frac{3}{2}} + S_{F,cv}^{t+\frac{1}{2}}}{2}\right]}_{(1)} \underbrace{S_{F,cv}^{t+1}}_{(2)} S_{O,cv}^{t+1} \exp\left(-\frac{T_a}{T_{cv}^{t+1}}\right). \tag{41}$$

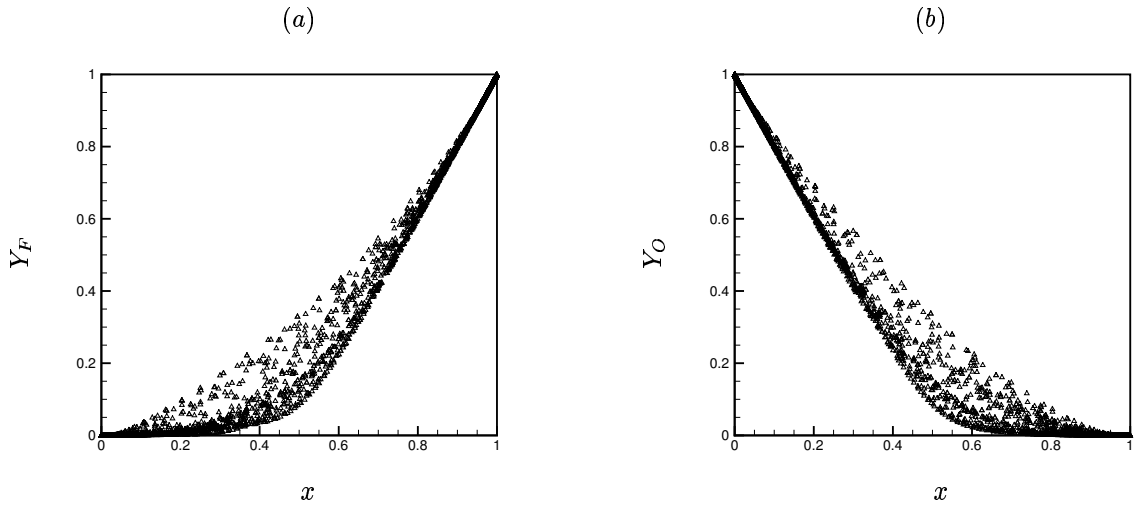

Figure 5. Scatter plot of (a) fuel mass fraction and (b) oxidizer mass fraction from DNS of one–step, turbulent/diffusion flame interaction. $Re = 935$, $Sc_k = Pr = 1$, $M_r = 0.1$.

The nonlinear source term is linearized by only solving for term (1) and treating term (2) as a coefficient. The outer loop ensures that the nonlinear corrections converge to zero. Note that the source terms in section D are linearized in the same manner.

IV. Results

The properties of the algorithm are first illustrated for a one dimensional steady laminar premixed flame and a unsteady laminar diffusion flame. These two examples will illustrate the ability to handle large heat release at low Mach number. The next validating case is a two dimensional laminar diffusion jet flame with large heat release at low Mach number. A three dimensional turbulent non–premixed flames with finite rate chemistry is then simulated. This problem accounts for turbulence at finite Mach number. The last case is the extension to complex chemistry incorporating a H2–O2 nine species, nineteen reaction mechanism.

A. 1D Laminar Premixed Flame and Laminar Diffusion Flame

The first reacting problem is a irreversible one–step laminar premixed flame. This problem tests the properties of large heat release and nearly incompressible reacting flow. For a premixed flame, the reaction is denoted as $R \rightarrow P$ where R is the reactant and P is the product.

For the laminar premixed flame, two source terms are considered. The Arrhenius model given by Williams[17] defined as:

$$\dot{\omega} = \Lambda \rho \left(1 - \Theta\right) \exp\left(\frac{-\beta \left(1 - \Theta\right)}{1 - \alpha \left(1 - \Theta\right)}\right). \tag{42}$$

The definition for α and β from Williams are $\alpha = \frac{T_2 - T_1}{T_2}$, $\beta = \frac{\alpha T_a}{T_2}$ and $\Lambda = B \exp\left(-\frac{\beta}{\alpha}\right)$.

The second source term is Echekki & Ferziger source term. The purpose of the Echekki and Feriger source term is that it approaches the Arrhenius source term, and is useful for validation, in that it permits analytical solution. Thus, Echekki & Ferziger[18] source term is defined as:

$$\dot{\omega} = \begin{cases} 0 & \text{for } \Theta < \Theta_c, \\ \beta \left(\beta - 1\right) \left(\Theta - 1\right) & \text{otherwise .} \end{cases} \tag{43}$$

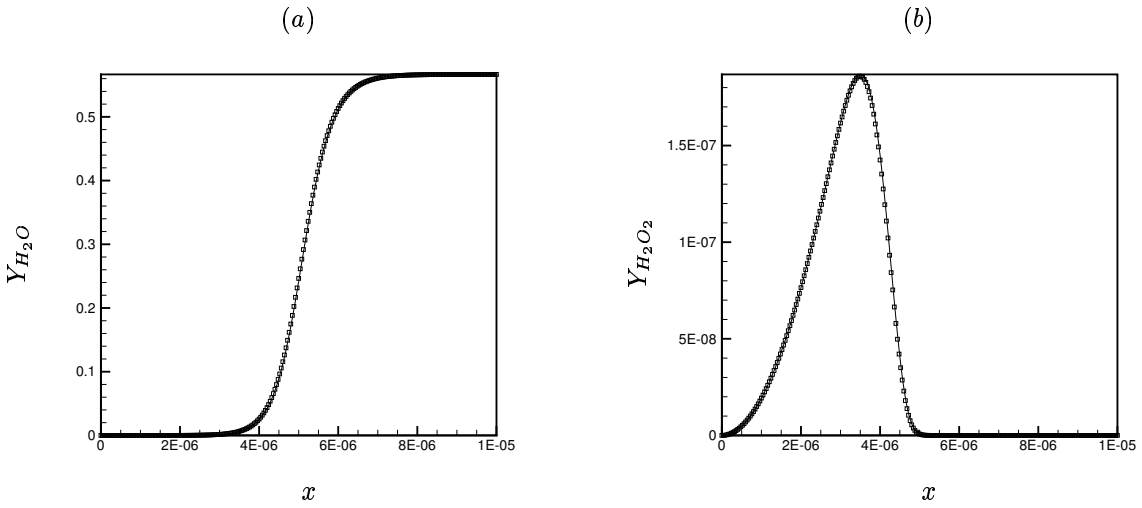

Figure 6. (a) This is a comparison between chemkin and the Code for a well–stirred reactor. (a) is a comparison between H_2O for a major species and (b) is a comparison between H_2O_2 for a minor species. □ Chemkin, ——— numerical solution.

Therefore, the analytical solution is defined as:

$$\Theta = \begin{cases} \left(1-\beta^{-1}\right)\exp\left(x\right) & \text{for } x \leq 0, \\ 1-\beta^{-1}\exp\left[\left(1-\beta\right)x\right] & \text{for } x \geq 0\ . \end{cases} \tag{44}$$

Note that a good value for β is around ten for a hydrocarbon reaction (Echekki & Ferziger[18]).

Figure 2 (a) is a comparison of the computed solution and the analytical solution where the Mach number is 0.01. Note that the computed and analytical solution agree well. Simulations were also performed for Arrhenius source term and similar results were obtained.

The next reacting case is a unstrained diffusion flame with a high Damkohler number ($Da = 50 \times 10^6$). A one–step irreversible diffusion flame developed by Cuenot & Poinsot [1] is modeled. The chemistry model is a one–step reaction defined as:

$$\nu_F Y_F + \nu_O Y_O \rightarrow \nu_P Y_P \tag{45}$$

where Y_F, Y_O and Y_P are the mass fractions of the fuel, oxidizer and products.

Cuenot & Poinsot [1] used an asymptotic method to derive expressions for the temperature and species profiles. This method can handle a diffusion flame with variable density, nonuniform Lewis number and finite rate chemistry. They studied unsteady unstrained, steady strained and unsteady strained $H_2 - O_2$ flames. Case 2 was the candidate to study because it has variable density and is an unsteady unstrained flame. Table 1 lists the condition for case 2.

Table 1. Test condition.

case	Le_F	$T_{F,0}$	Le_O	$T_{O,0}$	Φ	ν_F	ν_O	A	T_a	Q/c_p	Re
2	1	300 K	1	300 K	8	2	1	10^8	3600 K	6000 K	10000

Note that Le_F and Le_O denote the lewis number for fuel and oxidizer. $T_{F,0}$ and $T_{O,0}$ are the initial temperatures of the fuel and oxidizer. Φ is the equivalence ratio which is defined as:

$$\Phi = s\frac{Y_{F,0}}{Y_{O,0}} = \frac{\nu_O W_O}{\nu_F W_F}\frac{Y_{F,0}}{Y_{O,0}} \tag{46}$$

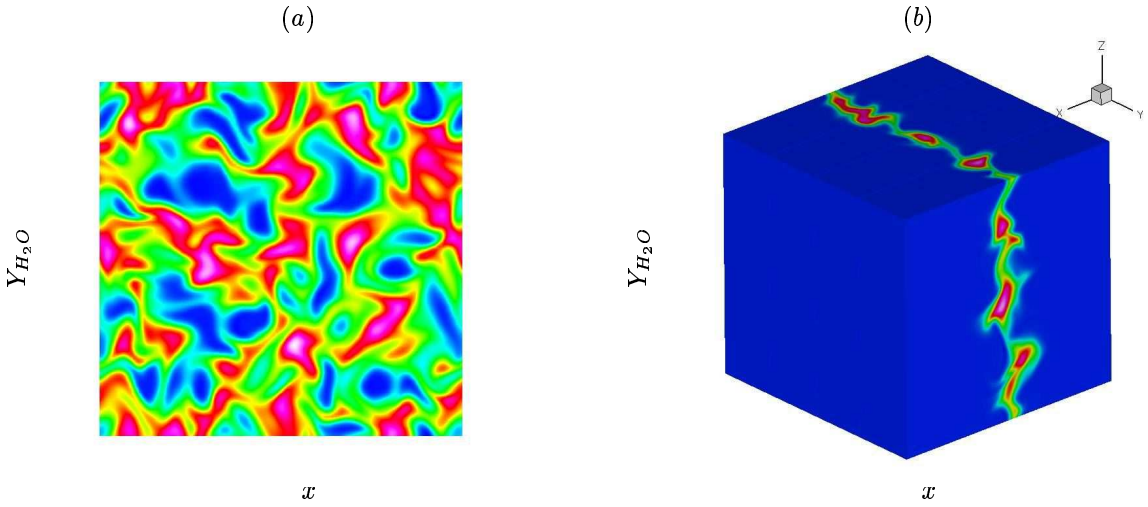

Figure 7. (a) is a slice in the middle of the flame showing the contour of the formation of H_2O and (b) is a contour plot of H_2O showing the entire computational domain

where s is the stoichiometric ratio. The equivalence ratio is used to determine if the mixture is rich, lean or stoichiometric. If $\Phi > 1$, the fuel mixture is rich and if $\Phi < 1$, then the mixture is lean.

For our test case, the Cuenot & Poinsot [1] asymptotic method was used for our initial condition where the time is initially at a non–dimensional time of 20. The simulations was advanced to a non–dimensional time of 64. Figure 2 (b) is a comparison of the computed solution to the asymptotic solution of oxidizer. The Mach number is 0.001 for this simulation and the grid is 512. Note that reasonable agreement is obtained between the computed and asymptotic solution.

B. 2D Laminar Diffusion Jet Flame

A steady two dimensional reacting laminar jet flame from Poinsot & Veynante[5] is computed. This problem illustrates the ability to handle large heat release and nearly incompressible flow. If one assumes constant mass flow rate (ρu =constant), $v = w = 0$ and $\rho D = constant$ then the mixture fraction ζ becomes the heat diffusion balance equation:

$$\rho_F u_f \frac{\partial \zeta}{\partial x} = \rho_F D_F \frac{\partial^2 \zeta}{\partial x^2}.$$

A similarity solution is obtained:

$$\zeta(x, y) = \frac{1}{2\sqrt{\pi \alpha x}} \exp\left(-\frac{y^2}{4\alpha x}\right)$$

where $\alpha = \frac{D_F}{u_F}$. A Hydrogen and Oxygen diffusion flame with Damkohler number of (50×10^6) was simulated. Figure 3 (a) shows the temperature contours of the simulation and figure 3 (b) is a comparison of the similarity solution to our simulation. The Mach number for this simulation is 0.01 and the grid is 128 by 128 where reasonable agreement is obtained.

C. 3D Turbulent non–premixed flames modeled with one-step chemistry

This example simulates a one–step diffusion flame interacting with three dimensional isotropic turbulence. The purpose of this calculation is to simulate isotropic turbulence interacting with one–step diffusion flames at finite Mach number. The results are compared to results from Mahalingam[20] and Chen.[21] The turbulence problem was simulated on a cubic domain with inflow and outflow boundary condition in the x–direction and periodic boundary condition in the y and z direction. The initial condition and parameters for the

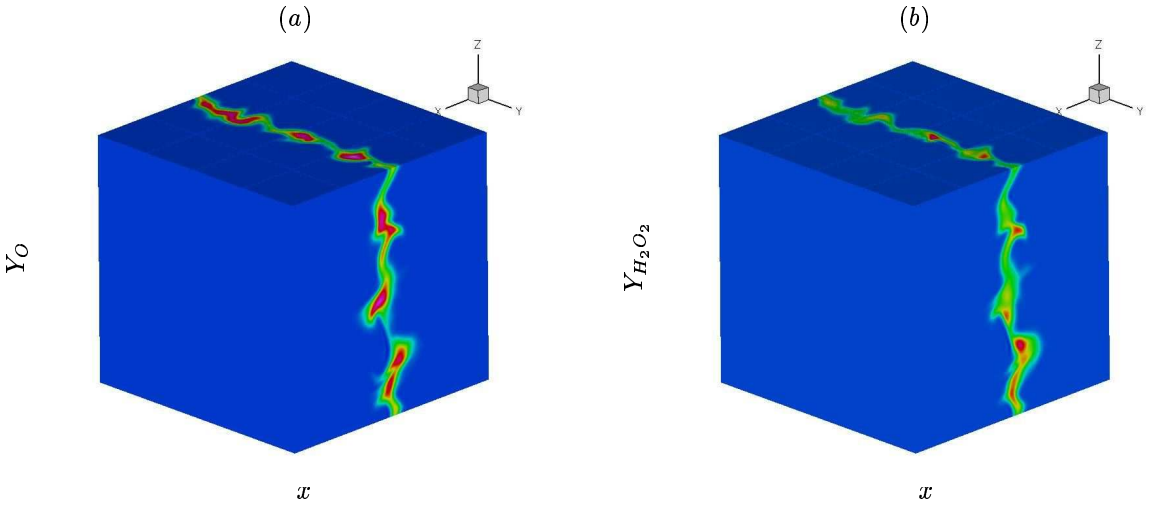

Figure 8. (a) is a 3D contour plot of O and (b) is a contour plot of H_2O_2

simulation are given in the table below. From table 3, z_{st} is defined as $z_{st} = \frac{1}{1+\Phi}$ where Φ is the equivalence

Table 2. Parameters for turbulence and flame.

β	α	ν_A	ν_B	Z_{st}	Re_λ	$\frac{L}{l_t}$	$\frac{l_t}{\delta_{fl}}$	$\frac{\eta}{\delta_{fl}}$	Da
8	0.8	1	1	0.5	50	6	2	0.2	1

ratio. ν_A and ν_B are the stoichiometric coefficients. A is the pre–exponential factor.

The initial turbulent kinetic energy spectrum is defined as:

$$E(k) = c_0 \frac{u_0^2}{k_0} \left(\frac{k}{k_0}\right)^4 \exp\left[-2\left(\frac{k}{k_0}\right)^2\right] \tag{47}$$

and the initial global Damkohler number is defined as:

$$Da = \frac{l_t}{u_0}\left[\frac{1}{\delta_{fl}}\int_{\delta_{fl}} \dot{\omega}\right]. \tag{48}$$

The diffusion flame was first advanced in time to remove the initial acoustic transients. Once the transients were removed, the turbulent velocity field was superimposed on the diffusion flame. The solution was advanced in time from 0 to 2.0 eddy turnover times and analyzed at each 0.1 eddy turnover time. The results show local extinction in the reaction rate. Holes occur in the reaction zones where pure mixing exists and from laminar flamelet theory, the holes location corresponds to a high rate of scalar dissipation rate (figure 4). Figure 5 shows two–dimensional mass concentration distribution of fuel mass fraction and oxidizer mass fraction. Reasonable agreement is obtained with Chen[21] (figure 2 (a) in their paper).

D. Modeling Complex Chemistry

This problem extends the algorithm to complex chemistry. The kinetic mechanism involving H_2 and O_2 is from *Mueller at el*,[19] and involves, 9 species and 19 reaction mechanism. Table 3 briefly lists the reaction mechanism. The solver was compared to Chemkin[29] for a well–stirred reactor problem to validate the

extension to complex chemistry. Figure 6 (a) is a comparison between H_2O mass fraction of our simulation to Chemkin for a major species and figure 6 (b) is a comparison of a minor species (H_2O_2). Note that good agreement is obtained. Also, this problem illustrates the purpose of handling the source terms implicitly. Comparison to explicit time advancement using the explicit euler method shows that dt was $1.0e-7$ for the explicit source term and $1.0e-2$ for implicit source term. For a large time step, the algorithm provided reasonable solution allowing one to take large time step while maintaining accuracy.

Table 3. Chemical Scheme: *Mueller*[19]

	Reaction	A_{fj}	β_j	E_j
1	$H + O_2 \rightleftharpoons O + OH$	$1.910E14$	0.0	16.44
2	$O + H_2 \rightleftharpoons H + OH$	$5.080E04$	2.67	6.29
3	$H_2 + OH \rightleftharpoons H_2O + H$	$2.160E08$	1.51	3.43
4	$O + H_2O \rightleftharpoons OH + OH$	$2.970E06$	2.02	13.4
5	$H_2 + M \rightleftharpoons H + H + M$	$4.580E19$	-1.40	104.38
6	$O + O + M \rightleftharpoons O_2 + M$	$6.160E15$	-0.5	0
7	$O + H + M \rightleftharpoons OH + M$	$4.710E18$	-1.0	0
8	$H + OH + M \rightleftharpoons H_2O + M$	$2.210E22$	-2.0	0
9	$H + O_2 + M \rightleftharpoons HO_2 + M$	$3.50E16$	-0.41	-1.12
10	$HO_2 + H \rightleftharpoons H_2 + O_2$	$1.660E13$	0.0	0.82
11	$HO_2 + H \rightleftharpoons OH + OH$	$7.080E13$	0.0	0.3
12	$HO_2 + O \rightleftharpoons OH + O_2$	$3.250E13$	0.0	0
13	$HO_2 + OH \rightleftharpoons H_2O + O_2$	$2.890E13$	0.0	-0.50
14	$HO_2 + HO_2 \rightleftharpoons H_2O_2 + O_2$	$4.200E14$	0.0	11.98
15	$H_2O_2 + M \rightleftharpoons OH + OH + M$	$1.20E17$	0.0	45.5
16	$H_2O_2 + H \rightleftharpoons H_2O + OH$	$2.410E13$	0.0	3.97
17	$H_2O_2 + H \rightleftharpoons H_2 + HO_2$	$4.820E13$	0.0	7.95
18	$H_2O_2 + O \rightleftharpoons OH + HO_2$	$9.550E06$	2.0	3.97
19	$H_2O_2 + OH \rightleftharpoons H_2O + HO_2$	$1.000E12$	0.0	0

Some preliminary results are shown in figure 7 extending section IV C to complex chemistry. The purpose of this problem is to study the effects of many time scales, and length scales associated with complex chemistry. Some preliminary results are shown in figures 7 and 8. Figure 7 (a) is slice in the middle of the flame showing the contour of the formation of H_2O and figure 7 (b) is a contour plot of H_2O showing the entire computational domain. Figure 8 (a) is a 3D contour plot of O and (b) is a contour plot of a minor species (H_2O_2).

V. Summary

This paper presents a non–dissipative, implicit, robust algorithm for direct numerical and large eddy simulation of compressible reacting flows. The method co–locates variables in space and time to allow easy extension to unstructured grids. The Navier–Stokes equations are non–dimensionalized using an incompressible scaling for pressure. From this scaling, the incompressible equations are recovered in the limit of zero Mach number and constant density. When the density varies, the zero Mach number equations for reacting flow are obtained. The discrete governing equations are discretely energy–conserving in the incompressible constant density limit (Hou & Mahesh[1]). The pressure, temperature, species and density are staggered in

time from the velocity. This allows the algorithm to be symmetric in time. The face normal velocity is obtained by projecting it to satisfy the energy equation. A pressure–projection approach is used. The energy equation therefore becomes an equation for the pressure correction. The algorithm uses central differences in time and space and is second order accurate. The species equations are implicit, and are solved separately to allow for easy extension to complex chemistry. Results are shown for premixed, diffusion flames and turbulent non–premixed flames. The numerical examples show the ability to handle chemical reaction in the limit of zero Mach number reacting flows and finite Mach number flows. The proposed method has attractive features for direct numerical and large eddy simulation of compressible reacting flows.

VI. Acknowledgments

This work was supported by the Air Force Office of Scientific Research under grant FA9550-04-1-0341 and the Department of Energy under the Stanford ASC alliance. Computing resources were provided by the Minnesota Supercomputing Institute, the San Diego Supercomputing Center and the National Center for Supercomputing Applications.

References

[1]Hou, Y., & Mahesh, K., 2005, A robust, colocated, implicit algorithm for direct numerical simulation of compressible, turbulent flows. *J. Comput. Phys.*, **205:** 205–221.

[2]Thompson, P.A., 1988, Compressible–fluid dynamics.

[3]Bijl, H. & Wesseling, P., 1998, A unified method for computing incompressible and compressible flows in boundary–fitted coordinates. *J. Comput. Phys.*, **141:** 153–173.

[4]Cuenot, B. & Poinsot, T., 1996, Asymptotic and numerical study of diffusion flames with variable Lewis number and finite rate chemistry. *Combust. Flame*, **104:** 111–137.

[5]Poinsot, T., & Veynante, D., 2001, Theoretical and Numerical Combustion. *Edwards.*

[6]Trouve, A., & Poinsot, T., 1994, The evolution equation for the flame surface density in turbulent premixed combustion. *J. Fluid Mech.*, **278:** 1–31.

[7]Lele, S. K., 1992, Compact finite difference schemes with spectral like resolution. *J. Comput. Phys.*, **103:** 16–42.

[8]Pantano, C., 2004, Direct simulation of non–premixed flame extinction in a methane–air jet with reduced chemistry. *J. Fluid Mech.*, **514:** 231–270.

[9]Majda, A. & Sethian J.A, 1985, The derivation and numerical solution of the equations for zero Mach number combustion. *Combust. Sci. Technol.* **42:** 185–205.

[10]Montgomery, C. J., G. Kosaly, and J. J. Riley., 1997, Direct numerical simulation of turbulent non–premixed combustion with multi–step hydrogen–oxygen kinetics, *Comb. Flame*, **109:** 113–144.

[11]Rutland, C. J. & Ferziger, J. H., 1990, Unsteady strained premixed laminar flames. *Combust. Sci. Tech.* **73:** 305.

[12]Rutland, C. J. & Ferziger, J. H., 1991, Simulations of flame–vortex interactions. *Combust. Flame* **84:** 343.

[13]Wall, C., Pierce, C. D., & Moin, P., 2002, A semi–implicit method for resolution of acoustic waves in low Mach number flows. *J. Comput. Phys.*, **181:** 545–563.

[14]Pember, R. B., Howell, L. H., Bell, J. B., Colella, P., Crutchfield, W. Y., Fiveland, W. A., & Jesse, J, P., 1997, An adaptive projection method for the modeling of unsteady, low-Mach number combustion. *Western States Section of the Combustion Institute.* 1997 Fall meeting.

[15]K. Mahesh, G. Constantinescu & P. Moin, 2004, A numerical method for large–eddy simulation in complex geometries. *J. Comput. Phys.* **197:** 215–240.

[16]Van der Heul, D.R., Vuik, C. & Wesseling, P., 2002, A conservative pressure–correction method for the Euler and ideal MHD equations at all speed. *Intnl. J. Num. Methods Fluids*, **40:** 521–529.

[17]Williams, F.A., 1985, Combustion Theory. *Benjamin Cummings.*

[18]Echekki, T. & Ferziger, J., 1993, A simplified reaction rate model and its application to the analysis of premixed flames. *Combust. Sci. Tech.*, **89:** 293–351.

[19]Mueller, M.A., Kim, T.J., Yetter, R.A., & Dryer, F.L., 1999, Flow Reactor Studies and Kinetic Modeling of the H2/O2 Reaction. *Int. J. Chem. Kinet.*, **31:** 113–125.

[20]Mahalingam, S., Chen, J., & Vervisch, L., 1995, Finite–rate chemistry and transient effects in direct numerical simulations of turbulent non-premixed flames. *Combust. Flame*, **102:** 285–297.

[21]Chen, J., Mahalingam, S., Puri, I. K., & Vervisch, L., 1992, Effect of finite–rate chemistry and unequal Schmidt number on turbulent non-premixed flames modeled with single-step chemistry. *CTR: Proceedings of the Summer Program 1992*: 367-387.

[22]Chen, J., Mahalingam, S., Puri, I. K., & Vervisch, L., 1992, Structure of turbulent non–premixed flames modeled with two-step chemistry. *CTR: Proceedings of the Summer Program 1992*: 389–402.

[23]Smooke, M., Mitchell., & Keyes, D., 1989, Numerical solution of two–dimensional axisymmetric laminar diffusion flames. *Comb. Sci. Tech.*, **67:** 85–121.

[24]Schlichting, H., 1968, Boundary–Layer Theory. *McGraw–Hill.*

[25]Wang, Y., & Trouve, A., 2004, Artificial acoustic stiffness reduction in fully compressible, direct numerical simulation of combustion. *Combust. Theory Modelling*, **8:** 633–659.

[26]Miller, H. P., Mitchell, R., Smooke, M & Kee, R., 1982, Towards a comprehensive chemical kinetic mechanism for the oxidation of acetylene: comparison of model predictions with results from flame and shock tube experiments. *19th Symp. (Int) on Combustion*: 181–196.

[27]Colonius, T., Moin, P. & Lele, S.K., 1995, Direct Computation of Aerodynamic Sound. *Report No. TF–65*, Department of Mechanical Engineering, Stanford Unverisity, Stanford, California.

[28]Turn, S. R., 2000, An Introduction to Combustion. *McGraw–Hill.*

[29]R. J. Kee, F. M. Rupley, J. A. Miller, M. E. Coltrin, J. F. Grcar, E. Meeks, H. K. Moffat, A. E. Lutz, G. Dixon-Lewis, M. D. Smooke, J. Warnatz, G. H. Evans, R. S. Larson, R. E. Mitchell, L. R. Petzold, W. C. Reynolds, M. Caracotsios, W. E. Stewart, P. Glarborg, C. Wang, C. L. McLellan, O. Adigun, W. G. Houf, C. P. Chou, S. F. Miller, P. Ho, P. D. Young, D. J. Young, D. W. Hodgson, M. V. Petrova, and K. V. Puduppakkam, CHEMKIN Release 4.1, Reaction Design, San Diego, CA (2006)